A single sensor dual-modality photoacoustic fusion imaging for compensation of light fluence variation

Jin, Haoran; Zhang, Ruochong; Liu, Siyu; Zheng, Zesheng; Zheng, Yuanjin

2019

Jin, H., Zhang, R., Liu, S., Zheng, Z., & Zheng, Y. (2019). A single sensor dual-modality photoacoustic fusion imaging for compensation of light fluence variation. IEEE Transactions on Biomedical Engineering, 66(6), 1810-1813. doi:10.1109/TBME.2019.2904502

https://hdl.handle.net/10356/143283

https://doi.org/10.1109/TBME.2019.2904502

A Single Sensor Dual-modality Photoacoustic Fusion Imaging for Compensation of Light Fluence Variation

Haoran Jin, Ruochong Zhang, Siyu Liu, Zesheng Zheng and Yuanjin Zheng*, *Senior Member*, *IEEE*

Abstract*— *Objective: **A photoacoustic signal is proportional to the product of the optical absorption coefficient and local light fluence; quantitative photoacoustic measurements of the optical absorption coefficients therefore require an accurate compensation of optical fluence variation. Usually, an additional diffuse optical tomography (DOT) is incorporated to estimate the light fluence variation, but it is often troubled with the bulky measurement system. On this note, we present a dual-modality photoacoustic fusion imaging method that is implemented with a normal photoacoustic imaging (PAI) device.** ***Methods:*** **A single piezoelectric transducer is employed to receive the photoacoustic waves and passive ultrasound (PU) waves simultaneously. Since the PU wave is generated by the backscattering and diffuse reflection photons, it has the capacity to facilitate diffuse reflectance (DR) imaging. We merged photoacoustic and DR imaging based on their dual-modality with a compensation of the optical fluence variation.** ***Results:*** **The absorption coefficient differences caused by the light fluence variation are reduced more than half with the proposed method, when comparing to the pure photoacoustic imaging.** ***Conclusion:*** **The dual-modality photoacoustic fusion imaging is able to correct the PAI errors caused by the optical fluence variation.** ***Significance:*** **The proposed method can be widely accepted by different PAI applications to compensate the light fluence variations without any additional required element.**

***Index Terms*— Photoacoustic imaging, Reflectometry, Image Fusion.**

I. Introduction

PHOTOACOUSTIC imaging (PAI) is an emerging technique based on the detection of ultrasonic waves excited in the studied medium due to the absorption of pulsed laser radiation by optical inhomogeneities. Hybrid nature of PAI allows it to combine spectral optical contrast and scalable acoustical resolution at millimetre to centimetre depths. These merits make PAI a practical tool for many applications in vascular, biology, oncology, neurology, ophthalmology, dermatology, gastroenterology, and cardiology [1]. To fulfil these different applications, PAI has developed many implementations e.g. molecular imaging [2], ocular imaging [3], and functional imaging [4] etc. However, the respected photoacoustic signal is a product of both the optical absorption coefficient (the quantity of interest) and the local light fluence. There is a concern that the backscattering and diffuse reflection effecting on spatial inhomogeneities may lead to the misinterpretation of photoacoustic images [5].

A non-invasive solution to this problem is combining PAI with diffuse optical tomography (DOT). Generally, the DOT system utilizes light in the near infrared spectral region to measure the optical absorption and scattering of physiological tissue, but DOT suffers with a low resolution. Taking the advantages of both PAI and DOT, a PAI/DOT dual-modality imaging can effectively compensate the light fluence variation to achieve accurate optical absorption coefficients. Such dual-modality imaging systems have been reported by several groups, following with some corresponding reconstruction methods for optical absorption [5-8]. However, these systems are more complicated than pure PAI systems, for they require additional fibres and sensors to receive and record photons.

Recently, a passive ultrasound (PU) technique is introduced into PAI, which uses passive elements to absorb laser energy to generate ultrasound waves [9-12]. The passive element can be defined as a small strong absorber; thus, it is convenient to integrate PU technique into a conventional PAI system. Besides appending an external absorber, a polyvinylidene difluoride (PVDF) film can also generate PU waves by absorbing backscattering lights. Based on this phenomenon, a new kind of PA/US imaging system is developed [13-15]. Mostly, PU techniques work as PA supplementary imaging for the structure analysis. Although PU technique can reveal some optical properties of materials [16-18], rare ones utilize it to compensate the light fluence variation.

In this letter, a single sensor dual-modality photoacoustic fusion imaging is proposed to correct the absorption coefficient differences caused by light fluence variation. As shown in Fig. 1, a laser beam shoots the scattering layer to generate reflection and transmission photons simultaneously. On one hand, the transmission photons are scattered in sample and absorbed by targets with photoacoustic waves generation. On the other hand, the reflection photons, caused by backscattering and diffuse reflection effects, are absorbed by a piezoelectric transducer and excite PU waves. Both the photoacoustic and PU waves are collected by the piezoelectric crystal in the transducer to form a photoacoustic and diffuse

The authors are with the School of Electrical and Electronic Engineering, Nanyang Technological University in Singapore, 50 Nanyang Avenue, Singapore 639798 (e-mail: hrjin@ntu.edu.sg).

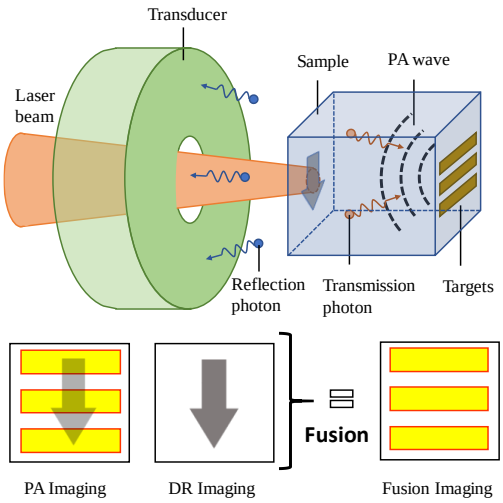

Fig. 1 The principle of photoacoustic fusion imaging.

reflectance (DR) dual-modality image. With these two images, the proposed fusion imaging is then approached by a reflection decoupling method.

II. Photoacoustic Setup

The dual-modality photoacoustic fusion imaging system is implemented as shown in Fig. 2(a). A pulse laser diode (Quantel) generates a 100*ns* duration pulse laser with 4*KHz* repetition frequency in a near-infrared spectrum (808*nm*), and the laser is delivered by a multimode fibre with a diameter of 400μm to our sensor head. After entering the sensor head, the laser sequentially passes through a reflect collimator (Thorlabs, RC02SMA-F01), a plane-convex lens (Thorlabs, LA1560-B-ML), a ring-shape transducer and finally illuminates on objects. The laser spot is weakly focused with a diameter of 2*mm* and a per-pulse energy of 56μJ. The custom-made ring-shape piezoelectric transducer (Doppler Ltd.) with a 2*MHz* centre frequency and a 20*mm* diameter is used to receive the PA and PU signals. In the transducer, a 5*mm* centre hole is designed to guarantee the laser beam travelling through. The distance between the object and the transducer surface is set as 9*mm*. For scanning imaging, an automation system moves the sensor head along the horizontal axes X and Y with a 50*Hz* repetition rate of laser pulses in an immersion chamber filled with distilled water. The stationary contact with the investigated object is ensured by the immersion chamber with a translucent window on the bottom made of a polyethylene film. At each scanning point, the signals are amplified by a 52*dB* preamplifier and averaged 10 times to reduce the noise.

For a phantom study, we use three black tapes as the objects placed at the bottom layer, and then two kinds of white plastic films marked as Film 1 and Film 2 cover on the objects being scattering layers as shown in Fig. 2(b). Both of the films backscatter much light energy, and the targets under them are difficult to be visualized by naked-eye. The minor differences on optical scattering properties can create the variations of penetrated light fluence. In Fig. 2(b), the shapes of the three stripe objects are outlined by dotted lines, and all the stripes have the same optical absorption coefficients. However, the PAI shown in Fig. 2(c) has large variances in optical absorptions under different scattering layers. The PAI result is plotted the top-down maximum value from 5μs to 10μs.

III. Passive Ultrasound

To compensate the light fluence variation, we should analyse the PU signal which is related to the diffuse reflectance. Generally, a piezoelectric transducer is composed of metal case, backing material, piezoelectric crystal, electrodes and matching layer as shown in Fig. 2(d). In such a structure, a backscattering light cannot directly illuminate on the piezoelectric conversion component, piezoelectric crystal, which is different to a PVDF-based detector. Rather, most of the light energies are absorbed by the matching layer, and the matching layer passively generates PU waves. There are two kinds of PU waves excited, the outward and inward PU waves. The outward PU wave propagates to the objects, which can be used as a standard pulse-echo ultrasound imaging for the structure supplementary of PA [15]. The inward PU wave propagates to the piezoelectric crystal and is then detected by the piezoelectric crystal. In our letter, we focus on the inward PU wave, and all the PU waves mentioned following represent the inward PU waves. To suppress the reverberation, the thickness of matching layer is usually designed as a quarter wavelength, thus the time flight of PU wave is only $T/4$ (Transducer oscillation period T). As the photoacoustic signal shown in Fig. 2(e), the photoacoustic wave is detected at time 6μs, while the PU wave is before 2μs. Fig. 2(f) zooms in the PU signal at range of 0μs - 2μs. Nevertheless, the PU wave is

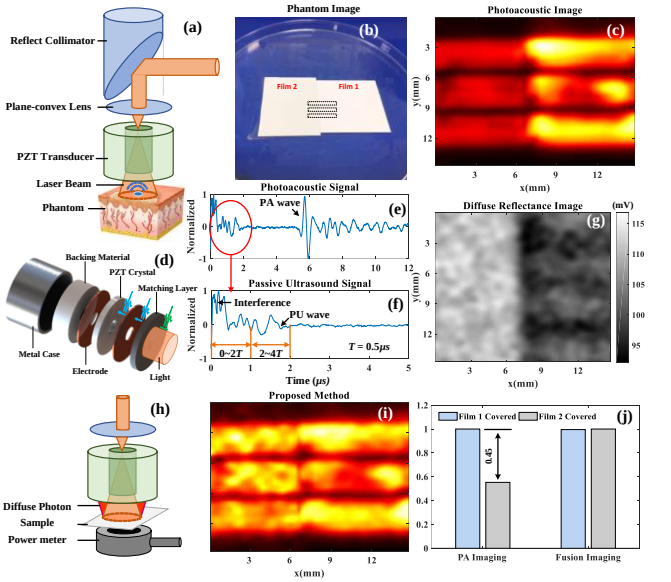

Fig. 2 (a) The experiment setup of photoacoustic fusion imaging. (b) The phantom photograph. The dot line outlines the object shape under the white films. (c) The raw photoacoustic image. (d) The generation of PU wave in a piezoelectrical transducer. The blue waves are inward PU waves. The green waves are outward PU waves. (e) The A-scan photoacoustic signal (f) The PU signal generated by backscattering light. (g) The diffuse reflectance image extracted from PU signals. (h) The calibration experiment setup. (i) The proposed fusion image. (j) The relative absorption coefficient of tapes. The blue and gray bars are the coefficients of objects covered by films 1 and 2, respectively.

overwhelmed by the laser coupling interference at $t = T/4$ ($T = 0.5\mu s$ for the $2MHz$ transducer), and difficult to extract directly. To avoid interference, we extract the PU wave at the time range of $t = 2T \sim 4T$, where the laser interference is greatly attenuated. A diffuse reflectance (DR) imaging can then be implemented by depicting the amplitude of PU wave in each scanning point. In our phantom experiment, the DR image is shown in Fig. 2(g) which approximates to the photograph of the scattering layer.

IV. Compensation Method

In a photoacoustic image, it directly reports the acoustic pressure distribution $p(\boldsymbol{r})$, arising from localized optical absorption. The acoustic pressure distribution can be simply defined as

$$p(\boldsymbol{r}) = \Gamma(\boldsymbol{r})h(\boldsymbol{r}), \tag{1}$$

where $\Gamma(\boldsymbol{r})$ is the Grueisen parameter and $h(\boldsymbol{r})$ is the heating function. Generally, the heating function is determined by a product of the optical absorption $\mu_a(\boldsymbol{r})$ and the light fluence $I(\boldsymbol{r})$ as

$$h(\boldsymbol{r}) = \mu_a(\boldsymbol{r})I(\boldsymbol{r}). \tag{2}$$

To fix the light fluence $I(\boldsymbol{r})$, we need the aid of PU wave. According to [19], the diffusion equation in a time-independent state is written as

$$I(\boldsymbol{r}) - \frac{1}{\mu_{eff}^2}\nabla^2 I(\boldsymbol{r}) = S(\boldsymbol{r})/\mu_a , \tag{3}$$

where μ_a is the absorption coefficient, and μ_{eff} is the effective attenuation coefficient defined as $\sqrt{3\mu_a(\mu_a + \mu_s')}$ where μ_s' is the reduced scattering coefficient. In our cases, the source term $S(\boldsymbol{r})$ is defined as $E - p_u(\boldsymbol{r})^2/\alpha$, where E is the whole light energy, $p_u(\boldsymbol{r})^2/\alpha$ denotes the energy of reflected photons and α represents the detection efficiency coefficient. Here, we use the 1-D diffusion case as a simplification, and its solution is

$$I(z) = \left(E - p_u{}^2/\alpha\right)\mu_{eff}e^{\left(-\mu_{eff}|z|\right)}\Big/2\mu_a . \tag{4}$$

Equation (4) can be rewritten in a form as

$$I = ap_u{}^2 + b, \tag{5}$$

where $a = -\mu_{eff}e^{\left(-\mu_{eff}|z|\right)}\Big/2\alpha\mu_a$ and $b = E\,\mu_{eff}e^{\left(-\mu_{eff}|z|\right)}\Big/2\mu_a$. In this experiment, all the targets are placed at the same depth for simplification, thus a and b is a constant for a specific scattering layer. A calibration experiment is used to estimate the parameters a and b . The setup of calibration experiment shown in Fig. 2(h) is similar to the photoacoustic imaging system but replaces the object with a laser power meter to record the energy of penetrated light. Firstly, the direct light fluence is recorded without penetrating any samples, which is about $56\mu J$. Then two plastic films used in the phantom experiment are tested. The energies of penetrated lights in Film 1 and Film 2 are about $19.5\mu J$ and $13.3\mu J$, respectively. Simultaneously, their amplitudes of PU waves (represent diffuse reflectance) are about $100mV$ and $115mV$, respectively. Based on the calibration results, the quadratic function is established between the penetrated light fluence and the PU wave amplitude.

After substituting (2) and (5) into (1), the optical absorption coefficient of the object is calculated by

$$\mu_a(\boldsymbol{r}) = p(\boldsymbol{r})\Big/\left[\left(ap_u(\boldsymbol{r})^2 + b\right)\Gamma(\boldsymbol{r})\right]. \tag{6}$$

Note that, the Gruneisen parameter $\Gamma(\boldsymbol{r})$ is assumed to be a constant in our experiments. Since this calculation of optical absorption coefficients combines photoacoustic image $p(\boldsymbol{r})$ and diffuse reflectance image (PU wave) $p_u(\boldsymbol{r})$, it is treated as a dual-modality photoacoustic fusion imaging. Benefiting from the compensation, the fusion imaging results show the uniform absorption coefficients of tapes in Fig. 2(i). Quantitively, the absorption coefficient differences caused by light backscattering are reduced from 0.45 in photoacoustic imaging to 0.03 in the proposed fusion imaging as shown in Fig. 2(j).

V. Ex-vivo Experiment

Further three ex-vivo trails on porcine tissues demonstrate the performance of the proposed method in biomedical applications. The experiment setup is similar to the phantom one, but the laser energy is $72\mu J$ per-pulse and the objects are defined by blue tapes with different shapes, including crossing, stripes and circle. Porcine tissues, mixed with lipids and muscles, cover on the objects to simulate the biomaterials with nonuniform optical scattering properties. All the porcine tissues are $1mm \sim 1.5mm$ in thickness and $9mm$ in distance to the transducer surface. The photographs of porcine tissues are depicted in Fig. 3(a)-(c) and the objects under the tissues are outlined using blue dotted lines. Since the optical diffuse reflectance of lipid is much stronger than muscle's, the penetrated light fluence obviously varies with the distributions of lipid and muscle. In such situations, the optical absorption coefficients estimated by PAI will be severely deteriorated. Fig. 3(e)-(g) show the photoacoustic images by displaying the top-down maximum values of photoacoustic signals at a range from $6\mu s$ to $10\mu s$. Although the shapes of objects can be recognized in PAI, the contrasts have large errors.

The DR image is illustrated by the maximum amplitudes in the time gate from 1 μs to 2 μs. In the DR images shown in Fig. 3(h)-(j), the bright areas indicate the lipid, and the dark ones represent the muscle tissue. It can be found that the shapes of lipid areas agree well with the ones defined in photographs.

Before using proposed fusion imaging, we should calibrate

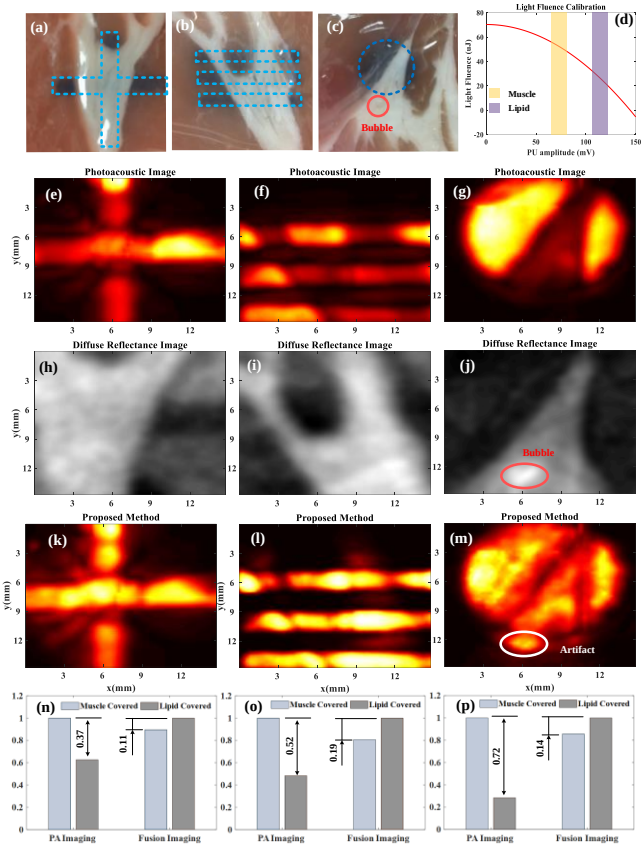

Fig. 3 (a) The photography of crossing object. (b) The photography of stripes object. (c) The photography of circle object. The shapes of objects are outlined using blue dotted lines. (d) Light fluences versus the amplitudes of PU waves. Yellow and purple bars indicate the amplitudes of PU waves generated from muscle and lipid tissues, respectively. (e) The PAI of crossing object. (f) The PAI of stripes object. (g) The PAI of circle object. (h) The diffuse reflectance imaging of crossing object. (i) The diffuse reflectance imaging of stripes object. (j) The diffuse reflectance imaging of circle object. (k) The fusion imaging of crossing object. (l) The fusion imaging of stripes object. (m) The fusion imaging of circle object. (n) The relative absorption coefficient of crossing object. (o) The relative absorption coefficient of stripes object. (p) The relative absorption coefficient of circle object. The blue and gray bars are the coefficients of objects covered by muscle and lipid tissues, respectively.

the relationship function between the penetrated light fluence and the amplitude of PU wave. According to the calibration results as shown in Fig. 3(d), we found that the penetrated light fluence and PU amplitude of lipid are about $30\mu J$ and $110.4mV$, respectively. For the muscle tissue, the penetrated light fluence increases to $50\mu J$, but the PU amplitude reduces to $74.6mV$.

Based on the calibrated relationship function, the distribution of optical absorption is obtained by (6), and the proposed fusion images are illustrated in Fig. 3(k)-(m). As a result, the fusion imaging corrects most errors existing in photoacoustic images. To quantitively compare the PAI and proposed fusion imaging, we calculate the relative absorption coefficients of objects and show the results in Fig. 3(n)-(p). The blue and gray bars represent the average absorption coefficients covered by muscle and lipid tissues, respectively. For PAI, the absorption coefficient differences are about 0.374, 0.517 and 0.716 in these three ex-vivo experiments. However, these differences are respectively reduced to 0.113, 0.193 and 0.144 in our proposed fusion imaging. More than half of the absorption coefficients differences are reduced.

VI. Discussions

Although the proposed fusion imaging can compensate the light fluence variation in most cases, some deficiencies should be clarified. One can find there is an artefact in Fig. 3(m) generated by a bubble. Since the bubble is not satisfied with the calibrated relationship function, it is not recognized and eliminated in the fusion image. Besides bubbles, the DR information acquired at the scattering layer boundary may be distorted. Since a finite size light focused spot covers both sides of scattering layers, the reflection photons are generated and mixed from both sides. It also indicates that the calibrated relationship function determines the accuracy of compensation, and media disobeys this function may result misleading results.

Two supplementary points should be noted here. In our proposed fusion imaging, we use a calibration method to estimate the relationship function between PU wave amplitude and penetrated light fluence. It is simple but may be not convenient for all applications. An alternative way is to use numerical models to calculate the numbers of reflection and transmission photons [20-22], and estimate the numbers of reflection photons absorbed by transducer statistically. Then, one can treat the PU waves as a diffuse reflectance meter to find the relationship function and utilize it to implement fusion imaging. The imaging resolution is another point should be stated. In this letter, the laser is weakly focused, and the transducer is flat; therefore, the imaging resolution is not high in our system. It is recommended to use strong focused laser beam (optical-resolution photoacoustic microscopy) [23] or focused transducer (acoustic-resolution photoacoustic microscopy) [24] to achieve a high resolution fusion imaging.

VII. Conclusion

In summary, we proposed a dual-modality photoacoustic fusion imaging method to compensate the optical absorption coefficient errors caused by backscattering and diffuse reflectance effects. The whole system is based on a single PAI device with a piezoelectrical transducer, thus, the imaging fusion can be implemented conveniently. Also, its concise design provides a great potential to integrate it with other scattering considered photoacoustic techniques [8, 25] to adapt for imaging with deep penetrations. According to the experiment results, the fused image greatly reduces the absorption coefficient differences caused by light fluence variations.

References

[1] L. Wang *et al.*, "A practical guide to photoacoustic tomography in the life sciences," *Nat. Methods*, vol. 13, no. 8, pp. 627-638, Jul. 2016.
[2] Q. Miao *et al.*, "Emerging Designs of Activatable Photoacoustic Probes for Molecular Imaging," *Bioconjugate Chem.*, vol. 27, no. 12, pp. 2808-2823, Nov. 2016.
[3] A. de la Zerda *et al.*, "Photoacoustic ocular imaging," *Opt. Lett.*, vol. 35, no. 3, pp. 270-272, Feb. 2010.
[4] J. W. Li *et al.*, "Functional Photoacoustic Imaging of Gastric Acid Secretion Using pH-Responsive Polyaniline Nanoprobes," *Small*, vol. 12, no. 34, pp. 4690-4696, Sep. 2016.
[5] L. Yin *et al.*, "Tomographic imaging of absolute optical absorption coefficient in turbid media using combined photoacoustic and diffusing light measurements," *Opt. Lett.*, vol. 32, no. 17, pp. 2556-2558, Sep. 2007.

[6] C. Xu *et al.*, "Investigation of a diffuse optical measurements-assisted quantitative photoacoustic tomographic method in reflection geometry," *J. Biomed. Opt.*, vol. 17, no. 6, p. 061213, May. 2012.
[7] P. D. Kumavor *et al.*, "Target detection and quantification using a hybrid hand-held diffuse optical tomography and photoacoustic tomography system," *J. Biomed. Opt.*, vol. 16, no. 4, p. 046010, Apr. 2011.
[8] A. Q. Bauer *et al.*, "Quantitative photoacoustic imaging: correcting for heterogeneous light fluence distributions using diffuse optical tomography," *J. Biomed. Opt.*, vol. 16, no. 9, p. 096016, Sep. 2011.
[9] B.-Y. Hsieh *et al.*, "All-optical scanhead for ultrasound and photoacoustic dual-modality imaging," *Opt. Express*, vol. 20, no. 2, pp. 1588-1596, Jan. 2012.
[10] J. Jose *et al.*, "Passive element enriched photoacoustic computed tomography (PER PACT) for simultaneous imaging of acoustic propagation properties and light absorption," *Opt. Express*, vol. 19, no. 3, pp. 2093-2104, Jan. 2011.
[11] T. F. Fehm *et al.*, "Four dimensional hybrid ultrasound and optoacoustic imaging via passive element optical excitation in a hand-held probe," *Appl. Phys. Lett.*, vol. 105, no. 17, p. 173505, Oct. 2014.
[12] J. L. Johnson *et al.*, "All-optical extravascular laser-ultrasound and photoacoustic imaging of calcified atherosclerotic plaque in excised carotid artery," *Photoacoustics*, vol. 9, pp. 62-72, Mar. 2018.
[13] P. Subochev *et al.*, "Simultaneous photoacoustic and optically mediated ultrasound microscopy: phantom study," *Opt. Lett.*, vol. 37, no. 22, pp. 4606-4608, Nov. 2012.
[14] P. Subochev *et al.*, "Simultaneous photoacoustic and optically mediated ultrasound microscopy: an in vivo study," *Biomed. Opt. Express*, vol. 6, no. 2, pp. 631-638, Feb. 2015.
[15] H. Jin *et al.*, "Passive ultrasound aided acoustic resolution photoacoustic microscopy imaging for layered heterogeneous media," *Appl. Phys. Lett.*, vol. 113, no. 24, p. 241901, Dec. 2018.
[16] P. Subochev *et al.*, "Simultaneous triple-modality imaging of diffuse reflectance, optoacoustic pressure and ultrasonic scattering using an acoustic-resolution photoacoustic microscope: feasibility study," *Laser phys. lett.*, vol. 13, no. 2, p. 025605, Jan. 2016.
[17] P. Subochev, "Cost-effective imaging of optoacoustic pressure, ultrasonic scattering, and optical diffuse reflectance with improved resolution and speed," *Opt. Lett.*, vol. 41, no. 5, pp. 1006-1009, Mar. 2016.
[18] P. Subochev *et al.*, "Simultaneous in vivo imaging of diffuse optical reflectance, optoacoustic pressure, and ultrasonic scattering," *Biomed. Opt. Express*, vol. 7, no. 10, pp. 3951-3957, Oct. 2016.
[19] L. V. Wang *et al.*, *Biomedical optics: principles and imaging*. John Wiley & Sons, 2012.
[20] S. L. Jacques, "Coupling 3D Monte Carlo light transport in optically heterogeneous tissues to photoacoustic signal generation," *Photoacoustics*, vol. 2, no. 4, pp. 137-142, Dec. 2014.
[21] K. D. Paulsen *et al.*, "Spatially varying optical property reconstruction using a finite element diffusion equation approximation," *Med. Phys.*, vol. 22, no. 6, pp. 691-701, Jun. 1995.
[22] V. Periyasamy *et al.*, "Advances in Monte Carlo simulation for light propagation in tissue," *IEEE Rev. Biomed. Eng.*, vol. 10, pp. 122-135, Aug. 2017.
[23] K. Maslov *et al.*, "Optical-resolution photoacoustic microscopy for in vivo imaging of single capillaries," *Opt. Lett.*, vol. 33, no. 9, pp. 929-931, May. 2008.
[24] J. Turner *et al.*, "Improved optoacoustic microscopy through three-dimensional spatial impulse response synthetic aperture focusing technique," *Opt. Lett.*, vol. 39, no. 12, pp. 3390-3393, Jun. 2014.
[25] M. J. Moore *et al.*, "Triplex micron-resolution acoustic, photoacoustic, and optical transmission microscopy via photoacoustic radiometry," *Opt. Express*, vol. 26, no. 17, pp. 22315-22326, Aug. 2018.